Numerical simulation of the combined effects of thermophoretic motion and variable thermal conductivity on free convection heat transfer

Muhammad Ashraf, Amir Abbas, Aamir Ali, et al.

View Online   Export Citation   CrossMark

ARTICLES YOU MAY BE INTERESTED IN
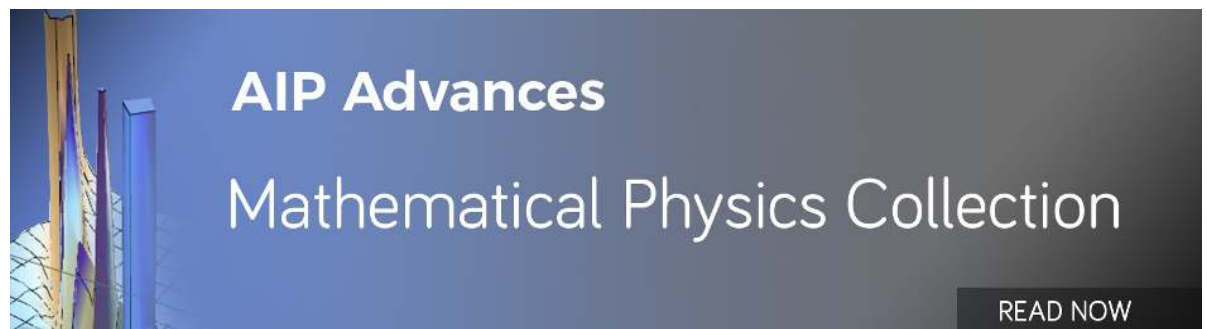
AIP Advances

Mathematical Physics Collection

READ NOW

Numerical simulation of the combined effects of thermophoretic motion and variable thermal conductivity on free convection heat transfer

Muhammad Ashraf,[1] (ID) Amir Abbas,[1] Aamir Ali,[2] (ID) Zahir Shah,[3] (ID) Hussam Alrabaiah,[4,5] (ID) and Ebenezer Bonyah[6,a] (ID)

AFFILIATIONS

[1] Department of Mathematics, Faculty of Science, University of Sargodha, Sargodha 40100, Pakistan
[2] Department of Mathematics, COMSATS University Islamabad, Attock Campus, Attock 43600, Pakistan
[3] Center of Excellence in Theoretical and Computational Science (TaCS-CoE), SCL 802 Fixed Point Laboratory, Science Laboratory Building, King Mongkut's University of Technology Thonburi (KMUTT), 126 Pracha-Uthit Road, Bang Mod, Thrung Khru, Bangkok 10140, Thailand
[4] College of Engineering, Al Ain University, Al Ain 64141, United Arab Emirates
[5] Department of Mathematics, Tafila Technical University, Tafila 66110, Jordan
[6] Department of Mathematics Education, University of Education, Winneba, Kumasi Campus, Kumasi 00233, Ghana

[a] Author to whom correspondence should be addressed: ebbonya@gmail.com

ABSTRACT

In the current research, the effect of thermophoretic motion combined with temperature-dependent thermal conductivity on natural convection flow around the surface of a sphere at several circumferential locations has been presented. The modeled nonlinear governing partial differential has been transformed into a dimensionless form with the help of appropriate non-dimensional variables. Later, the finite difference method is applied to solve the proposed model. The effect of controlling parameters, such as thermal conductivity variation parameter γ, Prandtl number Pr, Schmidt number Sc, thermophoretic coefficient k, and thermophoresis parameter N_t on the velocity field, temperature distribution, mass concentration, skin friction, rate of heat transfer, and rate of mass transfer has been highlighted. The estimations of the emerging parameters on the physical properties are displayed in graphical and in tabular forms. It has been predicted that the rise in γ, N_t, Sc, Pr, and k increases the velocity distribution, but the reverse behavior has been seen in the temperature field. The enhancement in N_t, Sc, Pr, and k boosts up the curves of mass concentration, and the rise in γ suppresses the concentration function. It has been observed that an increase in γ reduces the skin friction and the rate of mass transfer but opposite behavior of the rate of heat transfer occurs. Furthermore, increasing values of Sc cause the skin friction to lose the dominance in the rate of heat and mass transfer. It has been also noticed that increasing values of N_t strengthen the skin friction and rate of heat transfer, and attenuation occurs in the case of the rate of mass transfer.

NOMENCLATURE

ξ, η	primitive variables for velocity components in x and y directions	$C(\text{kg m}^{-3})$	mass concentration in boundary layer
		$C_P(\text{J kg}^{-1} \text{ K}^{-1})$	specific heat at constant pressure
a (m)	sphere's radius	$C_w(\text{kg m}^{-3})$	surface mass concentration
		$C_\infty(\text{kg m}^{-3})$	ambient mass concentration

$D_m\left(\text{m}^2\,\text{s}^{-1}\right)$ mass diffusion coefficient
$g\left(\text{m s}^{-2}\right)$ gravitational acceleration
k thermophoretic coefficient
N_t thermophoresis parameter
Pr   Prandtl number
Sc   Schmidt number
T (K)   fluid temperature in boundary layer
T_w(K)   surface temperature
T_∞(K)   temperature of the ambient fluid
U, V primitive variables for dimensionless axes X and Y
u, v x and y components of the velocity filed
$U_\infty\left(\text{m s}^{-1}\right)$ free stream velocity
V_t primitive variable for dimensionless thermophoretic velocity v_t
v_t dimensionless thermophoretic velocity

Greek symbols

$\beta_c\left(\text{K}^{-1}\right)$ concentration expansion coefficient
$\beta_t\left(\text{K}^{-1}\right)$ thermal expansion coefficient
γ thermal conductivity variation parameter

I. INTRODUCTION

The phenomenon observed in mixtures of moving submicron particles in which these particles move away or come toward the surface due to temperature gradient is termed nanoparticle motion commonly known as thermophoresis. This phenomenon takes place at the scale of 1 mm or even smaller. The force through which these particles gain the momentum is known as the thermophoretic force. Different types of particles give different responses to that force. Curl Ludwing was the first one to observe the thermophoresis in liquid mixtures in 1856, and in gas mixtures, it was reported in 1870. The thermophoretic force is used in the precipitators used commercially such as electrostatic precipitators. This can be used in the transport phenomenon of fouling. Thermophoresis has also been used to facilitate drug discovery. The thermophoretic force is used to separate the mixed particles. It has been used in dust-collecting devices, air pollution control, and capturing and removing small particles from the gas streams. There are other several practical applications in different fields. A mode of heat transfer that governs the fluid motion by density differences in the fluid due to the temperature gradient is termed free or natural convection. Natural convection and the thermophoresis phenomenon have motivated the research community due to their huge applications in engineering and natural sciences. Due to its significance in interdisciplinary research, we focus on the community engaged in this field. Epstein and Ellison[1] carried out the study of the correlations between the rate of aerosol deposition and instantaneous aerosol suspended species concentration. Particle deposition in the laminar tube flow in the presence of thermophoresis has been discussed by Park and Kim.[2] Chamkha and Pop[3] focused on the convective heat and fluid flow mechanism with the consideration of deposition effects over the vertical surface embedded in a porous medium. Rajabi[4] discussed the homotopy perturbation method for fin efficiency of convective straight fins with the contemplation of the influence of variable thermal conductivity. Attia[5] discussed the unsteady dusty fluid flow between two parallel

plates for variable thermal conductivity and viscosity. Grosan et al.[6] analyzed the effect of thermophoretic motion on fully developed free convection heat transfer in a vertical channel. Kuznetsov and Nield[7] studied the behavior of free convective heat transfer over a vertical plate for nanofluid. Özerinç et al.[8] examined the fully developed laminar forced convection flow through nano-fluids inside the circular tube under convective boundary conditions. Pal and Mondal[9] analyzed the mechanics of heat transfer in the presence of combined temperature-dependent viscosity, and Soret and Dufour effects. Kuznetsov and Nield[10] examined the revised model of the free convection boundary layer flow of nano-fluids over a vertical plate discussed in Ref. 7. Goodarzi et al.[11] investigated the heat and mass transfer phenomenon and the pressure drop mechanism in a corrugated surface heat exchanger by using the multiwalled carbon nanotubes in nanofluid. Goshayeshi et al.[12] performed the experimental study on the use of Fe_2C_3/kerosene nanofluid for the copper oscillating heat pipe under the effect of magnetic field. The effects of variable thermal conductivity and temperature-dependent viscosity in the presence of thermal radiation along the surface of the wedge have been concluded in Ref. 13. In this study, the authors claimed that the intensification of the estimations of the viscosity variation parameter or thermal conductivity increases the local skin friction coefficient and reduces the local Nusselt number. Ashraf et al.[14] proposed the model of convective flow over a magnetized surface by taking the effect of variable viscosity and temperature-dependent thermal conductivity. The effects of variable parameters on forced convection boundary layer flow along the permeable wedge have been illustrated by Alam et al.[15] numerically. Li et al.[16] discussed the model of force convection flow of the power-law of non-Newtonian fluid through semi-infinite parallel plates with the consideration of variable thermal conductivity. Malik et al.[17] studied the effect of variable thermal conductivity on heat transfer and fluid flow mechanism in Sisko fluid in the presence of an applied magnetic field. The characteristics of Williamson fluid in the energy mode for variable thermal conductivity and heat generation have been explored by Malik et al.[18] The effect of viscous dissipation on periodic mixed convection flow around a sphere has been simulated numerically by Ashraf et al.[19] Later, the solutions for time-dependent shear stress and heat transfer rate around various points of sphere associated with the fluid dissipation have been demonstrated in Ref. 20. Khan et al.[21] studied magneto-hydrodynamics heat and fluid flow principle of Carreu nanofluid with temperature-dependent thermal conductivity over a permeable stretching/shrinking sheet under the action of the heat source and sink. Alrashed et al.[22] proposed the model of laminar fluid flow and heat transfer of water/functional multiwalled carbon nanotube nanofluid. They used the finite volume method to solve the proposed model numerically. Later, Ashraf et al.[23] presented the nano-fluid heat transfer through natural convection around a sphere and in the plume region developed above the sphere. That work focused on the influence of the effective Prandtl number on the bio-convection flow of thermally developed magnetized tangent nanofluid with the incorporation of the slip flow condition and gyrotactic microorganisms in Ref. 24. Sheikholeslami et al.[25] considered the heat transfer mechanism in the ferro-fluid in the cavity having double moving walls by taking into account the effect of the electric field. The authors concluded that there is an augmentation in the temperature gradient corresponding to the enhancement in the electric force. Shah et al.[26] proposed the

study of the influence of viscous dissipation, Joule heating, and Hall current on the three-dimensional flow of couple stress nano-fluid past a surface stretching exponentially using the Cattaneo–Christov heat flux model. The natural convection flow process through the subclass of non-Newtonian nano-fluid known as the Casson nano-fluid along the surface stretching non-linearly has been presented by Ullah et al.[27] The authors encountered the effect of a magnetic field, Brownian motion, and thermophoresis under convective boundary conditions. Gheynani et al.[28] focused on the influence of diameter and concentration of nanoparticles on the material properties in non-Newtonian nanofluid through the three-dimensional micro-tube. They performed their study on the non-Newtonian carboxymethylcellulose and copper oxide nanofluid. Ghasemi et al.[29] used curve fitting and neutral network methods to investigate the experimental data related to nano-antifreezing containing carbon nanotubes for the prediction of thermal conductivity of the considered fluid by introducing two-variable correlation. Abbas et al.[30] examined the combined mechanism of mixed convection and thermophoretic transportation at different points around the surface of a sphere. Later, Abbas and Ashraf[31] studied the combined effects of mixed convection and thermophoresis on the physical properties with the inclusion of variable viscosities around the sphere. Some new related work can be studied in Refs. 32–35.

As a consequence of the above literature survey, it is noted that no attempt toward the study of combined effects of variable thermal conductivity and thermophoretic motion has been made so far. We have focused on the study of the physical behavior of the combined effects of nanoparticle motion and variable thermal conductivity on natural convection flow around a sphere for different values of parameters involved in the flow model, and they are displayed in tabular form as well as graphically.

II. MATHEMATICAL MODEL AND COORDINATE SYSTEM

This section demonstrates the representation of the physical model given in a schematic in Fig. 1. We consider two-dimensional, steady, viscous, and incompressible fluid flows around a sphere. The sphere is maintained at a temperature T_w and has a temperature greater than the surrounding temperature T_∞. In Fig. 1, the x-axis is taken along the surface of the sphere, the y-axis is considered normal to it, and $\bar{r}$ is the radial distance from the symmetric axis to the surface of a sphere, where a is the radius of the sphere. By following Ref. 30, the dimensionless boundary layer equations representing the heat and fluid flow model are given as

$$\frac{\partial(\sin xu)}{\partial x} + \frac{\partial(\sin xv)}{\partial y} = 0, \tag{1}$$

$$u\frac{\partial u}{\partial x} + v\frac{\partial u}{\partial y} = \frac{\partial^2 u}{\partial y^2} + \theta \sin x + \phi \sin x, \tag{2}$$

$$u\frac{\partial \theta}{\partial x} + v\frac{\partial \theta}{\partial y} = \frac{(1+\gamma\theta)}{Pr}\frac{\partial^2 \theta}{\partial y^2} + \frac{\gamma}{Pr}\left(\frac{\partial \theta}{\partial y}\right)^2, \tag{3}$$

$$u\frac{\partial \phi}{\partial x} + v\frac{\partial \phi}{\partial y} = \frac{1}{Sc}\frac{\partial^2 \phi}{\partial y^2} - \frac{\partial(v_t\phi)}{\partial y}. \tag{4}$$
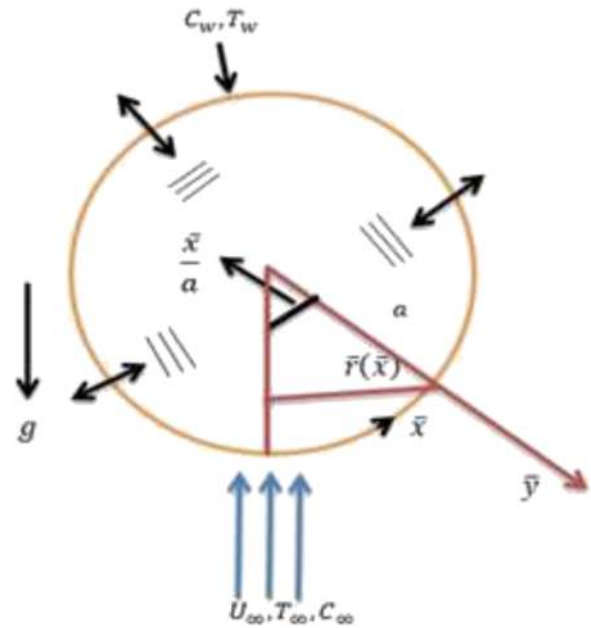

FIG. 1. Coordinate system and flow configuration.

The dimensionless variables are given as

$$x = \frac{\bar{x}}{a}, \ y = \frac{\bar{y}Gr^{\frac{1}{4}}}{a}, \ u = \frac{Gr^{-\frac{1}{2}}a\bar{u}}{v}, \ v = \frac{Gr^{-\frac{1}{4}}a\bar{v}}{v},$$

$$v_t = \frac{Gr^{-\frac{1}{4}}a\bar{v_t}}{v}, \ \theta = \frac{T-T_\infty}{T_w-T_\infty}, \ \phi = \frac{C-C_\infty}{C_w-C_\infty}, \tag{5}$$

$$\kappa = \kappa_\infty(1+\gamma^*\Delta T\theta).$$

Here, $Pr = \frac{v}{\alpha}$, $\gamma = \gamma^*\Delta T$, and $Sc = \frac{v}{D_m}$ are Prandtl number, thermal conductivity variation parameter with γ^* as a constant, and Schmidt number, respectively. The thermophoretic velocity appeared in Eq. (4) is expressed as

$$v_t = -\frac{k}{\theta + N_t}\frac{\partial \theta}{\partial y},$$

where $N_t = \frac{\Delta T}{T_\infty}$ and k represent the thermophoresis parameter and thermophoretic coefficient, respectively. The boundary conditions subject to the coordinate system are given as

$$u = 0, \ v = 0, \ \theta = 1, \ \phi = 1 \text{ at } y = 0,$$

$$u \to 0, \ \theta \to 0, \ \phi \to 0, \ \text{as } y \to \infty. \tag{6}$$

III. SOLUTION METHODOLOGY

The set of dimensionless governing equations (1)–(4) under associated boundary conditions expressed in Eq. (5) are transformed into a suitable form for integration by using suitable transformation

variables as follows:[23]

$$u(x,y) = x^{\frac{1}{2}} U(\xi,\eta), \ v(x,y) = x^{-\frac{1}{4}} V(\xi,\eta),$$
$$\eta = x^{-\frac{1}{4}} y, \ \xi = x, \ v_t(x,y) = x^{-\frac{1}{4}} V_t(\xi,\eta), \tag{7}$$
$$\theta(x,y) = \theta(\xi,\eta), \ \phi(x,y) = \phi(\xi,\eta).$$

The transformed system of field equations for further solutions is given as

$$\xi U \cos\xi + \left\{ \begin{array}{c} \xi \frac{\partial U}{\partial \xi} - \frac{1}{4}\eta \frac{\partial U}{\partial \eta} \\ + \frac{1}{2}U + \frac{\partial V}{\partial \eta} \end{array} \right\} \sin\xi = 0, \tag{8}$$

$$\xi U \frac{\partial U}{\partial \xi} + \frac{1}{2}U^2 + \left(V - \frac{\eta U}{2}\right)\frac{\partial U}{\partial \eta} = \frac{\partial^2 U}{\partial \eta^2} + \theta \sin\xi + \phi \sin\xi, \tag{9}$$

$$\xi U \frac{\partial \theta}{\partial \xi} + \left(V - \frac{\eta U}{2}\right)\frac{\partial \theta}{\partial \eta} = \frac{(1+\gamma\theta)}{Pr}\frac{\partial^2 \theta}{\partial \eta^2} + \frac{\gamma}{Pr}\left(\frac{\partial \theta}{\partial \eta}\right)^2, \tag{10}$$

$$\xi U \frac{\partial \phi}{\partial \xi} + \left(V - \frac{\eta U}{2}\right)\frac{\partial \phi}{\partial \eta} = \frac{1}{Sc}\frac{\partial^2 \phi}{\partial \eta^2} - \frac{\partial(V_t \phi)}{\partial \eta}, \tag{11}$$

where $V_t = -\frac{k}{\theta + N_t}\frac{\partial \theta}{\partial \eta}$.

The corresponding transformed boundary conditions are given as

$$U = 0, \ V = 0, \ \theta = 1, \ \phi = 1, \ \text{at } \eta = 0,$$
$$U \to 0, \ \theta \to 0, \ \phi \to 0 \ \text{as } \eta \to \infty. \tag{12}$$

IV. NUMERICAL PROCEDURE

The set of dimensionless transformed equations (8)–(12) is approximated by the finite difference technique, the central difference along the y-axis, and the backward difference along the x-axis from where we obtain the following system of the algebraic form of the conservation equations:

$$V_{i+1,j} = \left\{ V_{i-1,j} - 2\xi_i \frac{\Delta\eta}{\Delta\xi}(U_{i,j} - U_{i,j-1}) + \frac{1}{4}\eta_j(U_{i+1,j} - U_{i-1,j}) - \Delta\eta U_{i,j} \right\}$$
$$\times 2\Delta\eta \xi_i \frac{\cos\xi_i}{\sin\xi_i} U_{(i,j)}, \tag{13}$$

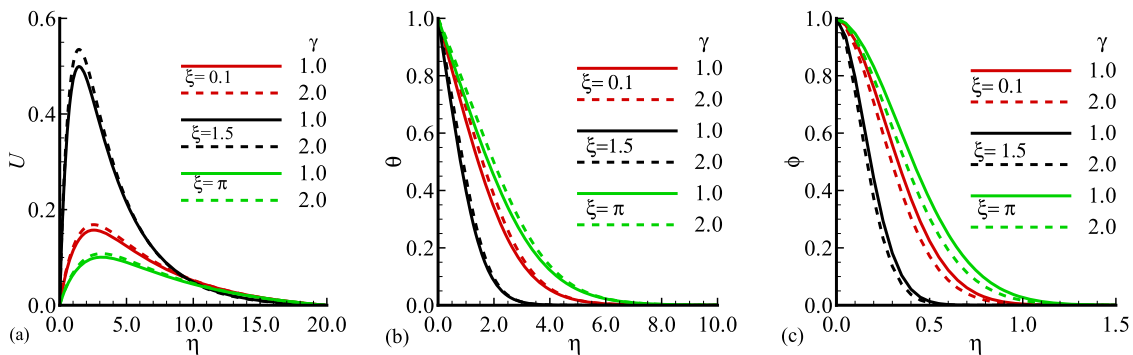$$A_1 U_{(i-1,j)} + B_1 U_{(i,j)} + C_1 U_{(i+1,j)} = D_1, \tag{14}$$

$$A_2 \theta_{(i-1,j)} + B_2 \theta_{(i,j)} + C_2 \theta_{(i+1,j)} = D_2, \tag{15}$$

$$A_3 \phi_{(i-1,j)} + B_3 \phi_{(i,j)} + C_3 \phi_{(i+1,j)} = D_3. \tag{16}$$

Here, $A_1, B_1, C_1, A_2, B_2, C_2, A_3, B_3$, and C_3 are coefficient matrices, and the discretized thermophoretic velocity is

$$V_{t(i,j)} = -\frac{k}{(\theta_{(i,j)} + N_t)}\frac{\theta_{(i+1,j)} - \theta_{(i-1,j)}}{2\Delta\eta}.$$

The corresponding boundary conditions are

$$U_{(i,j)} = 0, \ V_{(i,j)} = 0, \ \theta_{(i,j)} = 1, \ \phi_{(i,j)} = 1, \ \text{as } \eta_j = 0,$$
$$U_{(i,j)} \to 0, \ \theta_{(i,j)} \to 0, \ \phi_{(i,j)} \to 0,$$
$$\eta_j \to \infty. \tag{17}$$

Here, $U_{(i,j)}, \theta_{(i,j)}$, and $\phi_{(i,j)}$ are unknown physical quantities representing velocity, temperature, and mass concentration profiles, respectively. The derivatives of the above mentioned material properties around a sphere at different locations are also computed and then tabulated. We solved Eqs. (13)–(16) and the boundary conditions (17) by using the Gaussian elimination technique numerically. We use Fortran-95, and, then, the obtained data are uploaded by using Techplot-360 to generate graphs.

V. NUMERICAL RESULTS AND DISCUSSION

In this section, we the highlight the graphical and tabular form of the effect of several dimensionless numbers such as thermophoresis parameter, N_t, Schmidt number, Sc, thermophoretic coefficient, k, thermal conductivity variation parameter, γ, and Prandtl number, Pr, on the velocity field, U, temperature field, θ, and mass concentration, ϕ. Furthermore, the effect of these parameters is also estimated by skin friction, $\frac{\partial U}{\partial \eta}$, rate of heat transfer, $\frac{\partial \theta}{\partial \eta}$, and rate of mass transfer, $\frac{\partial \phi}{\partial \eta}$, along the prescribed geometry. Figures 2(a)–2(c) present the effect of various values of γ on flow velocity, temperature field, and mass concentration. We can observe that as γ is increased, the velocity distribution and temperature field are increased but mass concentration is reduced for the same variations of γ at the same positions.

FIG. 2. Graphs of physical quantities (a) U, (b) θ, and (c) ϕ for various values of γ, when Pr = 7.0, Sc = 10.0, Nt = 20.0, and k = 1.0.

It is noteworthy that the velocity of the fluid exhibits prominent growth behavior at point $\xi = 1.5$ for $\gamma = 2.0$. On the other hand, temperature field and mass concentration obtain maximum values for $\gamma = 2.0$ and $\gamma = 1.0$ at the same position $\xi = 0.1$, respectively. This behavior was expected because an increase in γ is due to the high temperature difference according to the definition of γ, which helps the fluid to conduct more heat resulting in the rise in temperature of the fluid flow domain. The enhancement in the temperature of the fluid flow as water is considered lessens the fluid viscosity; hence, the velocity of the fluid flow domain augments. Figures 3(a)–3(c) illustrate the difference in the behavior of quantities, U, θ, and, ϕ, for, $N_t = 1.0, 20.0$. It is noted that the velocity field and the mass concentration grow significantly and the temperature field declines with very minor difference when N_t is drastically increased. Results show that the velocity field contribution is prominent for $\xi = 1.5$. The temperature and mass distributions are notably very near to the leading edge, that is, at $\xi = 0.1$. It confirms to the reality that as N_t is augmented, the temperature gradient takes the increasing effects, which provoke the submicron particles causing the intensification in flow velocity and mass concentration. The numerical results of the velocity field, temperature field, and mass distribution for diverse values of Pr are illustrated graphically in Figs. 4(a)–4(c). It is noted that the velocity field and mass concentration increase with increasing

Prandtl number, but no significant change is observed in temperature distribution for the same variations and at the same points. Furthermore, the increasing behavior of velocity is not for $\xi = 1.5$, but the other two quantities maintain their largest values at a trailing point $\xi = \pi$. Physically, for this phenomenon, it is true because an increase in Pr is due to a decrease in thermal conductance of the fluid that leads to a decrease in the temperature distribution with minor difference.

Figures 5(a)–5(c) display the results for material quantities, U, θ, and ϕ for Sc = 1.0, 50.0 at three different points. It is worthy to note that enhancement in Sc increases U and ϕ, but dilutes the effectiveness of θ. Furthermore, the attitude of velocity participation in flow field is dominant in this range of appropriate choice of the above said parameter at location $\xi = 1.5$; but, on the other hand, the temperature and mass distributions are dominant at the trailing edge. On the ground of physical reasoning, this phenomenon supports the arguments that increase in Sc is due to the decrease in the mass diffusion coefficient causing the reduction in resistance. Therefore, this reduced resistance allows the fluid to maximize its speed and consequently enhance the mass concentration. The numerical solutions of main quantities, U, θ, and ϕ for diverse values of k, are displayed in Figs. 6(a)–6(c). In these figures, substantial enhancement in the velocity field and the mass concentration is observed, but reverse
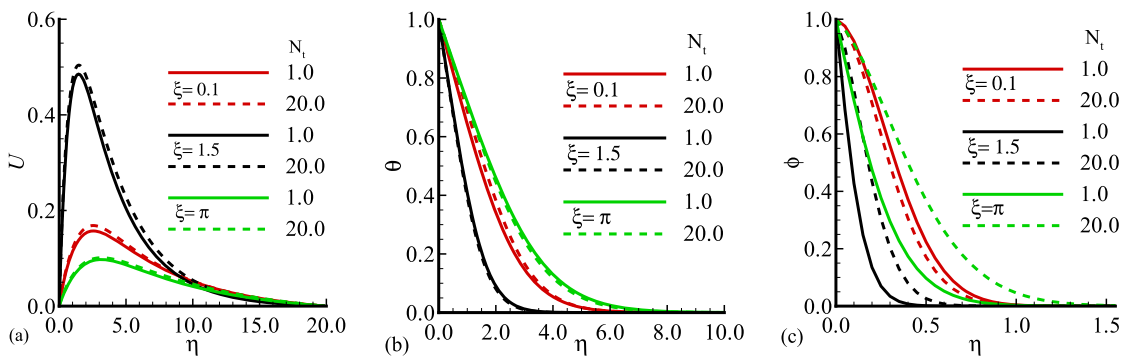

FIG. 3. Graphs of physical quantities (a) U, (b) θ, and (c) ϕ for various values of N_t, when Pr = 7.0, Sc = 2.0, $\gamma = 0.2$, and $k = 1.0$.
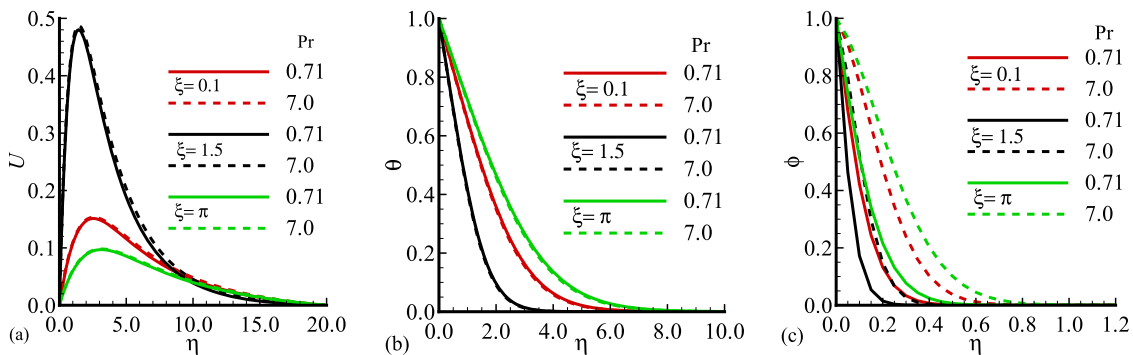

FIG. 4. Graphs of physical quantities (a) U, (b) θ, and (c) ϕ for various values of Pr, when Sc = 10.0, $\gamma = 0.05$, $N_t = 20.0$, and $k = 1.0$.
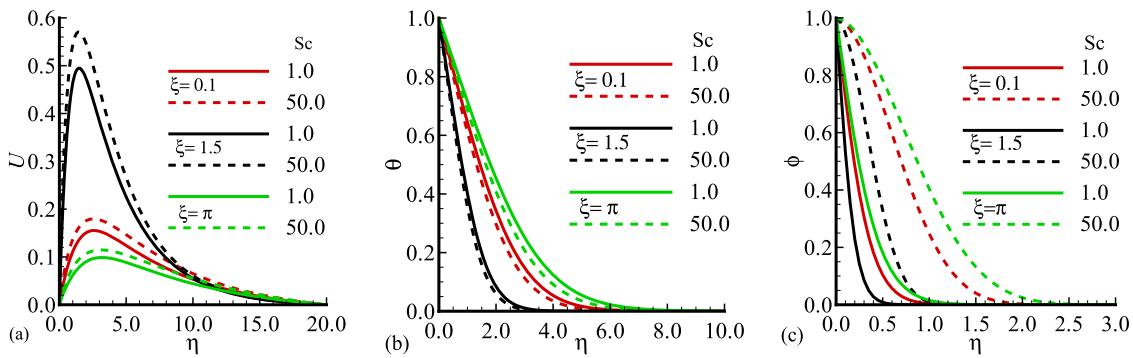
FIG. 5. Graphs of physical quantities (a) U, (b) θ, and (c) ϕ for various values of Sc, when Pr = 7.0, γ = 0.8, N_t = 20.0, and k = 2.0.
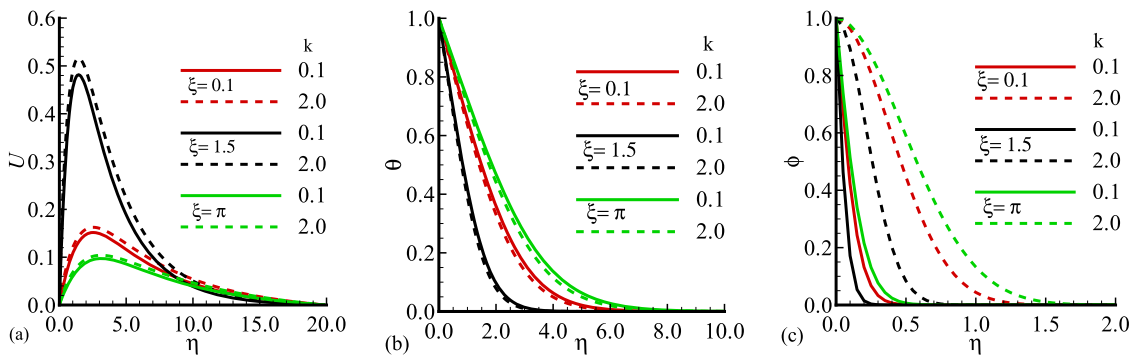

FIG. 6. Graphs of physical quantities (a) U, (b) θ, and (c) ϕ for various values of k, when Pr = 7.0, Sc = 10.0, γ = 0.4, and N_t = 20.0.

behavior in the temperature field is seen as k is increased. Moreover, it can be noted that the velocity field has the maximum value at point ξ = 1.5. Temperature and mass distributions obtain maximum at point ξ = π in the fluid flow regime. Physically, it is valid that an increase in the thermophoretic coefficient incites the submicron particles to move with greater thermophoretic velocity that leads to increase in the mass concentration. Table I shows the numerical results for the chief physical quantities, $\frac{\partial U}{\partial \eta}$, $\frac{\partial \theta}{\partial \eta}$, and $\frac{\partial \phi}{\partial \eta}$, for

sundry values of γ at stations ξ = 0.1, 1.0, 1.5, 2.0, 2.5, π of a sphere. In Table I, it is concluded that quantities $\frac{\partial U}{\partial \eta}$ and $\frac{\partial \phi}{\partial \eta}$ are increased, while $\frac{\partial \theta}{\partial \eta}$ reduces with an increase in γ. It is a point of interest to note that all of the three aforementioned quantities obtain maximum values at locations ξ = 1.5, 2.0. Table II illustrates the numerical results for the same properties mentioned earlier in Table I for the same values of Sc around different locations of a sphere. Table II

TABLE I. Numerical solutions for physical quantities $\frac{\partial U}{\partial \eta}$, $\frac{\partial \theta}{\partial \eta}$, and $\frac{\partial \phi}{\partial \eta}$ for various values of γ at different points on the sphere, when N_t = 20.0, Sc = 10.0, k = 1.0, and Pr = 7.0.

	$\left(\frac{\partial U}{\partial \eta}\right)_{\eta=0}$		$\left(\frac{\partial \theta}{\partial \eta}\right)_{\eta=0}$		$\left(\frac{\partial \phi}{\partial \eta}\right)_{\eta=0}$	
ξ	γ = 0.1	γ = 2.0	γ = 0.1	γ = 2.0	γ = 0.1	γ = 2.0
0.1	0.324 72	0.325 33	0.478 26	0.472 83	0.000 34	0.000 35
1.0	1.606 70	1.609 68	0.815 28	0.806 02	0.000 52	0.000 54
1.5	1.825 27	1.828 66	0.850 71	0.841 04	0.000 54	0.000 56
2.0	1.702 87	1.706 03	0.831 24	0.821 80	0.000 53	0.000 55
2.5	1.244 39	1.246 70	0.748 68	0.740 17	0.000 49	0.000 51
π	0.168 21	0.168 52	0.383 90	0.379 54	0.000 27	0.000 28

TABLE II. Numerical solutions for physical quantities $\frac{\partial U}{\partial \eta}$, $\frac{\partial \theta}{\partial \eta}$, and $\frac{\partial \phi}{\partial \eta}$ for various values of Sc at different points on the sphere, when $N_t = 20.0$, $k = 2.0$, and γ and Pr = 7.0.

ξ	$\left(\frac{\partial U}{\partial \eta}\right)_{\eta=0}$		$\left(\frac{\partial \theta}{\partial \eta}\right)_{\eta=0}$		$\left(\frac{\partial \phi}{\partial \eta}\right)_{\eta=0}$	
	$Sc = 1.0$	$Sc = 50.0$	$Sc = 1.0$	$Sc = 50.0$	$Sc = 1.0$	$Sc = 50.0$
0.1	0.367 47	0.330 33	0.523 87	0.483 72	0.000 85	0.000 01
1.0	1.818 25	1.634 42	0.892 98	0.822 49	0.001 40	−0.000 01
1.5	2.065 60	1.856 76	0.931 80	0.860 42	0.001 45	−0.000 01
2.0	1.927 08	1.732 24	0.910 47	0.840 73	0.001 42	−0.000 01
2.5	1.408 25	1.265 86	0.820 03	0.757 22	0.001 30	0.000 00
π	0.190 24	0.171 11	0.420 45	0.388 29	0.000 69	0.000 01

TABLE III. Numerical solutions for physical quantities $\frac{\partial U}{\partial \eta}$, $\frac{\partial \theta}{\partial \eta}$, and $\frac{\partial \phi}{\partial \eta}$ for various values of N_t at different points on the sphere, when $Sc = 2.0$, $k = 1.0$, $\gamma = 0.2$, and Pr = 7.0.

ξ	$\left(\frac{\partial U}{\partial \eta}\right)_{\eta=0}$		$\left(\frac{\partial \theta}{\partial \eta}\right)_{\eta=0}$		$\left(\frac{\partial \phi}{\partial \eta}\right)_{\eta=0}$	
	$N_t = 1.0$	$N_t = 20.0$	$N_t = 1.0$	$N_t = 20.0$	$N_t = 1.0$	$N_t = 20.0$
0.1	0.282 47	0.341 24	0.456 81	0.503 67	0.306 11	0.001 71
1.0	1.397 09	1.688 12	0.778 63	0.858 45	0.523 19	0.000 283
1.5	1.587 08	1.917 76	0.812 47	0.895 76	0.546 12	0.002 94
2.0	1.480 68	1.789 16	0.793 88	0.875 25	0.533 52	0.002 88
2.5	1.082 13	1.307 46	0.715 03	0.788 32	0.480 14	0.002 62
π	0.146 32	0.176 79	0.366 69	0.404 41	0.245 63	0.001 38

predicts that quantities $\frac{\partial U}{\partial \eta}$, $\frac{\partial \theta}{\partial \eta}$, and $\frac{\partial \phi}{\partial \eta}$ are reduced as Sc is increased. It is interesting to note that these quantities obtain the maximum values at positions $\xi = 1.5$. Table III demonstrates the results of the same material properties considered in previous two tables for $N_t = 1.0, 20.0$ at several points $\xi = 0.1, 1.0, 1.5, 2.0, 2.5$, and π. It is observed that as N_t is intensified, the reduction in the rate of mass transfer is seen at all the chosen locations. Interestingly, the rate of heat transfer and the skin friction increase under the same parametric conditions at the same circumferential points. All of the three quantities are at the peak position at $\xi = 1.5$.

VI. CONCLUDING REMARKS

In the current study, the effect of nanoparticles' motion along with temperature-dependent thermal conductivity on free convection flow around the surface of a sphere is taken for investigation numerically. The characteristics of the velocity field, temperature field, and mass distribution, as well as skin friction heat transfer rate and mass transfer rate for different controlling parameters are examined. The findings of our numerical results of the proposed model are outlined in this section. It is predicted that the velocity field increases with increasing values of γ, N_t, Sc, Pr, and k. The velocity distribution obtains a maximum value at the position $\xi = 1.5$. The temperature field increases as γ increases and decreases when Sc

and k increase. No significant changes in the behavior of the temperature field are seen at points $\xi = 0.1, 1.5$, and π as Pr and N_t are increased. The mass concentration decreases as γ is increased but increases for the increasing values of N_t, Pr, Sc, and k. Mass concentration is prominent at $\xi = 0.1$ for various values of γ and N_t. It is maximum at $\xi = \pi$ for various values of Pr, Sc, and k. It is noted that all three aforementioned quantities obtain highest values at $\xi = 1.5$.

It is concluded that the skin friction, rate of heat transfer, and mass transfer rate reduce as Sc is increased, and the growth of these quantities is maximum at $\xi = 1.5$. It is observed that as N_t is enhanced, attenuation takes place in the mass transfer rate, and the reverse phenomenon occurs for the skin friction and the heat transfer rate. All three quantities reach peak positions at $\xi = 1.5$.

ACKNOWLEDGMENTS

DATA AVAILABILITY

The data that support the findings of this study are available from the corresponding author upon reasonable request.

REFERENCES

[1] M. Epstein and P. G. Ellison, Nucl. Eng. Des. **107**, 327 (1988).

[2] S. H. Park and S. S. Kim, Int. J. Heat Mass Transfer **36**, 3477 (1993).

[3] A. J. Chamkha and I. Pop, Int. Commun. Heat Mass Transfer **31**, 421 (2004).

[4] A. Rajabi, Phys. Lett. A **364**, 33 (2007).

[5] H. A. Attia, Commun. Nonlinear Sci. Numer. Simul. **13**, 1077 (2008).

[6] T. Grosan, R. Pop, and I. Pop, Heat Mass Transfer **45**, 503 (2009).

[7] A. V. Kuznetsov and D. A. Nield, Int. J. Therm. Sci. **49**, 243 (2010).

[8] S. Özerinç, A. G. Yazıcıoğlu, and S. Kakaç, Int. J. Therm. Sci. **62**, 138 (2012).

[9] D. Pal and H. Mondal, J. Magn. Magn. Mater. **331**, 250 (2013).

[10] A. V. Kuznetsov and D. A. Nield, Int. J. Therm. Sci. **77**, 126 (2014).

[11] M. Goodarzi, A. Amiri, M. Karimipour, E. M. Laguri, and M. Dahari, Int. Commun. Heat Masss Transfer **66**, 172 (2015).

[12] H. R. Goshayeshi, M. Goodarzi, and M. Dahari, Exp. Therm. Fluid Sci. **68**, 663 (2015).

[13] W. Cai, N. Su, and X. He, J. Appl. Math. Comput. **52**, 305 (2016).

[14] M. Ashraf, A. J. Chamkha, S. Iqbal, and M. Ahmad, Int. J. Numer. Methods Heat Fluid Flow **26**, 1580 (2016).

[15] M. S. Alam, M. A. Khatun, M. M. Rahman, and K. Vajravelu, Int. J. Mech. Sci. **105**, 191 (2016).

[16] B. Li, W. Zhang, and L. Zhu, J. Phys.: Conf. Ser. **745**, 032035 (2016).

[17] M. Y. Malik, A. Hussain, T. Salahuddin, M. Awais, and S. Bilal, AIP Adv. **6**, 025316 (2016).

[18] M. Y. Malik, M. Bibi, F. Khan, and T. Salahuddin, AIP Adv. **6**, 035101 (2016).

[19] M. Ashraf, A. Fatima, and R. S. R. Gorla, Can. J. Phys. **95**, 976 (2017).

[20] M. Ashraf and A. Fatima, J. Heat Transfer **140**, 701 (2018).

[21] M. Khan, M. Irfan, L. Ahmad, and W. A. Khan, Phys. Lett. A **382**, 2334 (2018).

[22] A. A. A. A. Alrashed, O. A. Akbari, A. Heydari, D. Toghraie, M. Zarringhalam, G. A. S. Shabani, A. R. Seifi, and M. Goodarzi, Physica B **537**, 176 (2018).

[23] M. Ashraf, A. Khan, and R. S. R. Gorla, Heat Transfer—Asian Res. **48**, 1127 (2019).

[24] Y. Wang, H. Waqas, M. Tahir, M. Imran, and C. Y. Jung, IEEE Access **7**, 130008 (2019).

[25] M. Sheikholeslami, Z. Shah, A. Tassaddiq, A. Shafee, and I. Khan, IEEE Access **7**, 21048 (2019).

[26] Z. Shah, A. Dawar, E. O. Alzahrani, P. Kumam, A. J. Khan, and S. Islam, IEEE Access **7**, 64844 (2019).

[27] I. Ullah, K. S. Nisar, S. Shafie, I. Khan, M. Qasim, and A. Khan, IEEE Access **7**, 93076 (2019).

[28] A. R. Gheynani, O. A. Akbari, M. Zarringhalam, G. A. S. Shabani, A. A. Alnaqi, M. Goodarzi, and D. Toghraie, Int. J. Numer. Methods Heat Fluid Flow **29**, 1699 (2019).

[29] A. Ghasemi, M. Hassani, M. Goodarzi, M. Afrand, and S. Manafi, Physica A **514**, 36–45 (2019).

[30] A. Abbas, M. Ashraf, Y.-M. Chu, S. Zia, I. Khan, and K. S. Nisar, Molecules **25**, 2694 (2020).

[31] A. Abbas and M. Ashraf, "Combined effects of variable viscosity and thermophoretic transportation on mixed convection flow around the surface of a sphere," Therm. Sci. (published online).

[32] O. A. Akbari, M. R. Safaei, M. Goodarzi, N. S. Akbar, M. Zarringhalam, G. A. S. Shabani, and M. Dahari, Adv. Powder Technol. **27**, 2175–2185 (2016).

[33] M. Safaei, H. Togun, K. Vafai, S. Kazi, and A. Badarudin, Numer. Heat Transfer, Part A **66**, 1321–1340 (2014).

[34] S. Islam, A. Khan, W. Deebani, E. Bonyah, N. A. Alreshidi, and Z. Shah, AIP Adv. **10**, 055015 (2020).

[35] Z. Shah, L. B. McCash, A. Dawar, and E. Bonyah, AIP Adv. **10**, 065137 (2020).